Electrochimica Acta 348 (2020) 136291

Contents lists available at ScienceDirect

Electrochimica Acta

journal homepage: www.elsevier.com/locate/electacta

Unraveling the contributions of internal resistance components in two-chamber microbial fuel cells using the electrode potential slope analysis

Ruggero Rossi , Bruce E. Logan *

Department of Civil and Environmental Engineering, The Pennsylvania State University, 231Q Sackett Building, University Park, PA, 16802, USA

ARTICLE INFO

Article history:
Received 3 March 2020
Received in revised form
13 April 2020
Accepted 22 April 2020
Available online 25 April 2020

Keywords:
Two-chamber BES
Electrode resistance
Solution resistance
H-cell MFCs

ABSTRACT

Two-chamber (H-cell) bioelectrochemical systems (BESs) are one of the most widely used devices in bioelectrochemistry studies, but comparisons of performance have been challenged by differences in reactor architecture. Here we showed that the reactor solution resistance should be calculated using only the tube cross-sectional area and length rather than the electrode spacing (i.e. the solution resistance in the chambers is negligible). This approach was demonstrated using two H-cells (tube cross sectional areas of 4.5 cm^2 or 1.2 cm^2) and variable electrode areas. The solution resistance (R_Ω) calculated from the tube diameter and length was consistent with that measured using electrochemical impedance spectroscopy (EIS), and was ~80% of the total internal resistance with electrode areas larger than the tube area. Anode resistance and total power were similar ($R_{An} = 26 \pm 1\ \Omega$ to $R_{An} = 34 \pm 1\ \Omega$, 0.37 ± 0.00 mW) when the anode was larger than the tube area (4.5 cm^2), but the resistance increased ($R_{An} = 431 \pm 229\ \Omega$) when the anode size (0.8 cm^2) was smaller than the tube. Power and cathode resistance changed more with the size of the cathode ($R_{Cat} = 61 \pm 5\ \Omega$ at 9.6 cm^2, to $R_{Cat} = 73 \pm 7\ \Omega$ at 4.9 cm^2), with very high resistance when the cathode was smaller than the tube diameter ($R_{Cat} = 1246 \pm 805\ \Omega$ for 0.8 cm^2 cathode). These results demonstrated that internal resistances are relatively insensitive to electrode sizes when the electrodes are larger than the tube area. While it has not been common to report tube geometry in H-cell studies, these dimensions will need to be reported in future studies in order to make practical comparisons of performance among these types of reactors.

1. Introduction

Exoelectrogenic microorganisms drive electricity generation in microbial fuel cells (MFCs) through oxidation of organic matter in solution [1]. MFCs can be made with relatively inexpensive materials and simple configurations [2], [–] [5] but the lack of standardized conditions have led to results that cannot be directly compared due to reactor configuration differences [6,7]. MFC architectures vary widely, ranging from simple two-chamber bottle reactors connected by small side arms (H-cells), to plate and frame (equally sized electrodes) and tubular configurations [6,8]. Anodes are usually made of carbon-based materials, such as carbon felt, carbon cloth, graphite rods and graphite brush electrodes [9], with modifications often made to these materials to improve power production [9–13]. The electron acceptor in the cathodic chamber is typically oxygen provided by aeration or by direct air transfer, but chemical catholytes such as ferricyanide have also been used [1,6,14]. The variations in all of these system conditions have made it difficult to judge whether claims of increased power production, for example due to the treatment of electrodes, could instead be due to different architectures or materials in the test conditions over time, or low power production by controls (electrodes prior to modifications). Even when experimental conditions and reactor setups are identical, MFC performance has been shown to vary by ~15%, due to the techniques used by different investigators, electrode deterioration, and biofilm development [7].

Two-chamber, H-cell configurations are one of the more common architectures used in MFC tests, with performance typically evaluated in terms of the maximum power from polarization tests normalized to the area of one electrode [1,7,9,15]. In polarization tests, the external resistance is progressively reduced at regular intervals of time. While this is a common method for evaluating the

* Corresponding author.
E-mail address: blogan@psu.edu (B.E. Logan).

https://doi.org/10.1016/j.electacta.2020.136291
0013-4686/

overall performance of the reactor, it does not properly take into account the impact of the individual components of the internal resistance on the overall MFC performance. For example, it was reported that the anode working potential at the maximum power density in seven independent studies varied over a range of 267 mV in polarization tests [15]. Moreover, there is no clear rationale or standard for choosing the area for normalizing the power, and claims of high power densities in these systems has resulted in controversial findings upper limits in power production, especially when comparing results from H-cells to MFCs with different configurations [1,16]. For example, power densities have been reported to exceed 5 W m^{-2} in a 2018 H-cell study with a large anode (12.7 cm long, ~4.5 cm diameter brush anode) and a much smaller cathode (5 × 5 mm) in a ferricyanide catholyte, with power normalized to the smaller cathode [17]. The use of ferricyanide may help growing strictly anaerobic exoelectrogens, as its use can avoid oxygen leaking into the anolyte, but ferricyanide catholyte inflates power densities with respect to aerated catholytes due to its larger functional electrochemical potential than oxygen [18–20]. H-cells typically use electrodes suspended in the chamber with a proton exchange membrane (PEM) in the tube separating the chambers, with the electrode and tube sizes that vary between different studies. Normalizing the current or power to a smaller electrode can exaggerate the maximum performance relative to MFCs with equally-sized electrodes and cross sectional area between them, suggesting higher overall power production than that possible by the whole system [21].

The performance of electrodes in MFCs can individually be evaluated with proper location and use of reference electrodes, but often MFC performance is only reported in terms of whole cell polarization data without electrode potential results. A recently developed method to quantify the electrode and solution resistances and the working electrode potentials, called the electrode potential slope (EPS) analysis, was recently developed to quantify the performance of components in single chamber MFCs [15,22]. The slopes of linearized electrode polarization data were used to quantify the anode and cathode resistances, while the intercepts on the electrode potential axis defined the effective half-cell potentials at current near the maximum power. When the electrodes have the same cross sectional area as the chamber separating the electrodes the solution resistance can be calculated from the solution conductivity, and electrode area and spacing. Thus, it is possible in these systems to evaluate individual electrode performance through the EPS analysis, separate from ohmic losses due to solution resistance.

Previous applications of the EPS method required that the electrodes have the same size and their cross sectional area be the same as that of the chamber between them. However, H-cells do not meet these criteria and thus it has not been clear on how the analysis could be applied to these configurations due to the different (an usually smaller) tube cross sectional area than the projected areas of the electrodes (i.e. a small diameter tube connecting the much larger electrode chambers), different projected areas (and sometimes shapes) of the electrodes, different lengths of the connecting tube, and the use of different catholytes. All of these differences impact the overall total internal resistance and thus the maximum power possible in these systems [23–26]. A critical missing factor in this analysis was how the solution resistance could be calculated from a standard conductivity-solution resistance equation for the H-cell design given the different areas of the electrodes and membrane, and the distances of the electrodes from each other in addition to variable tube diameter and lengths.

Using electrochemical impedance spectroscopy (EIS), we demonstrate here that electrode performance in H-cells (for certain conditions) can be analyzed by using different assumptions in the EPS method for these cells compared to assumptions made for equally sized electrodes and chambers. This modified method is based on changing the approach used to calculate the solution resistance. While both approaches require calculation of the solution conductivity, the EPS method applied to H-cells requires the use of the diameter and length of the side arms. This utility of this new approach for H-cells was tested by using two different tube cross sectional areas, and by individually varying the size of one electrode relative to the other one. While various tests have previously been performed using H-cells with different dimensions, many studies did not report essential data needed for this analysis on the individual electrode potentials and geometry [17,19,20,23]. We also propose a method to report power production normalized to area, based on the projected areas of the system that contribute to internal resistances, in order to be able to better compare results using different H-cell configurations.

2. Materials and methods

2.1. Construction and operation of MFCs

The MFCs used here were two chamber, H-cell type reactors constructed from two bottles each with a side arm tube (Fig. S1A), with a PEM (Nafion 117, Fuel Cell Store, USA) clamped between the two chambers. The tube areas were either 1.2 cm^2 (small tube MFC; ST-MFC) or 4.5 cm^2 (large tube MFC; LT-MFC). The volume of the media in each bottle was slightly different, with 275 mL (4.5 cm^2 tube) or 260 mL (1.2 cm^2 tube), due to the different volumes of the side arms. The distance between the electrodes was 14 cm, and the total length of the two connected tubes was 7.5 cm.

Anodes (9.6 cm^2 initial projected area) were 6.35 mm thick carbon felt (Alfa Aesar, USA), heat treated at 450 °C for 30 min [27] prior to use. Pt/C cathodes were prepared as previously described [28]. Briefly, 35 mg Pt/C (10 wt %, E-TEK) and 467 μL Nafion ionomer (5 wt % solution, Dupont, USA) were vortexed with 233 μL isopropanol and painted on one side of a carbon cloth (Fuel Cell Earth, USA) (9.6 cm^2 projected area). The cathodes were then dried overnight in an oven (60 °C). The final Pt loading (0.5 mg cm^{-2}) was determined by normalizing the weight difference before and after catalyst coating by the projected area of the electrode. Anodes and cathodes were connected to a titanium wire current collector using electrically conductive carbon cement (Leit-C™, SPI supplies, German) [29].

The electrodes were positioned in the middle of the bottle chamber facing each other at ~3 cm from the side arm. Reference electrodes (REs) (Ag/AgCl; model RE-5B, BASi, IN; +0.209 V versus a standard hydrogen electrode, SHE) used to measure the anode and cathode potentials were placed in each chamber outside the electric field [30] at ~2 cm from the working electrode. To investigate the impact of the electrode dimension on the MFC performance the anode or cathode projected areas were progressively reduced for one electrode, from 9.6 cm^2, 7.1 cm^2, 4.9 cm^2, 3.1 cm^2, 1.8 $cm^2$and 0.8 cm^2 immediately before the polarization tests, while keeping the counter electrode a constant size (Fig. S1B). Additional tests were conducted after acclimating the 0.8 cm^2 anode at low external resistance (200 Ω) for two additional days.

The anolyte was 50 mM phosphate buffer solution (PBS; 4.58 g Na_2HPO_4, 2.45 g NaH_2PO_4, 0.31 g NH_4Cl, 0.13 g KCl in 1 L of distilled water, with 12.5 mL of a concentrated trace mineral solution and 5 mL of a vitamin solution) amended with sodium acetate (2 g L^{-1}) having a conductivity of $\sigma = 7.9$ mS cm^{-1} and pH = 7.0 ± 0.1. The catholyte was 50 mM phosphate buffer (PB; 4.58 g Na_2HPO_4, 2.45 g NaH_2PO_4) at pH = 7.0 ± 0.1 with conductivity of $\sigma = 6.3$ mS cm^{-1}. The catholyte was sparged with air at 17 ± 3 L h^{-1} and both chambers were continuously mixed using a magnetic stirrer. The

MFCs were operated at 30 °C in a controlled temperature room.

2.2. Electrochemical measurements

MFCs were acclimated at an external resistance of 1000 Ω as previously described [10]. The reactors were fed with fresh media in batch mode over several weeks, until at least 3 reproducible and stable voltage profiles were obtained [20]. Single cycle polarization tests were conducted once stable operation were reached by feeding the reactor with fresh media and maintaining the system at open circuit conditions for 2 h, and then steadily reducing the external resistance from 50,000, 10,000, 5000, 2000, 1000, 500, 200, 100 to 50 Ω at 20 min intervals.

The current was calculated based on the potential (E_{cell}) measured across the external resistor, and recorded using a computer based data acquisition system (2700, Keithley Instrument, OH). During each polarization test, the anode (E_{An}) and cathode (E_{Cat}) potentials were recorded using the reference electrodes in each chamber [23]. The electrode potentials measured between the working electrode and the RE in the opposite chamber (including the solution resistance) are included in the Supporting Information. All potentials are reported here versus SHE.

The EPS method was used to examine the performance of the MFC [15]. For this method, the electrode potentials from polarization curves were plotted with respect to current after correction for the solution resistance, and the linearized portion of the electrode potential at a current range when the maximum power occurs was used to quantify anode and cathode performance. The slope of the electrode potential was used to calculate individual electrode resistance, and the intercept on the *y*-axis was used to define the effective half-cell potential under working experimental conditions [15,22]. The linearized portion of the electrode potential in polarization plots, as a function of current, was fitted by $E = m\ i + b$, where i is the current (mA), the absolute value of the slope m is defined as the resistance of the anode (R_{An}) or cathode (R_{Cat}) in units of Ω, and the *y*-intercepts are used to calculate the experimental open circuit potentials of the anode ($E_{An,e0}$) or cathode ($E_{Cat,e0}$). A schematic representation of the parameters used for the EPS analysis is reported in the Supporting Information (Fig. S2). Using the linearized portion of the electrode potential near the maximum power, it is possible to reproduce the power density curve in polarization tests (Fig. S14) [15].

EIS measurements were used to determine the solution resistance between the electrodes. Tests were conducted using a two electrode setup at a constant applied potential of 0.54 V (tube = 4.5 cm^2) and 0.36 V (tube = 1.2 cm^2), corresponding to the E_{cell} generated at 1000 Ω, over a frequency range of 100 kHz to 5 mHz. For the MFCs with the 0.8 cm^2 electrodes (anode or cathode) the applied potential was reduced to 0.40 V (LT-MFC) and 0.30 V (ST-MFC) as the reactors were unable to sustain stable currents at such high potentials for the timeframe necessary to obtain the spectra. A sinusoidal perturbation of 10 mV amplitude was applied registering 10 points per decade. Prior to the analysis the whole cell potential was set to the potential correspondent to the EIS analysis for 30 min. The spectra were then analyzed and fitted into the equivalent circuits reported in the Supporting Information (Fig. S3, Fig. S4, Table S1, and Table S2) to determine the solution resistance ($R_Ω$).

2.3. Estimating solution resistance from solution conductivity

The solution resistance ($R_Ω$) obtained from EIS was compared with that calculated from the solution conductivity (σ, mS/cm), as

$$R_Ω = \frac{10^3 l}{\sigma A} \quad (1)$$

where A is the cross-sectional area between the electrodes (cm^2), 10^3 is to convert mS into S (where 1 S = Ω^{-1}) and l is the length of the electric path (cm) [23]. In H-cell MFCs, the appropriate length of the electric path or the cross-sectional area of the electric field cannot be easily predicted. For example, it is not clear whether the electrode area or the tube area will better represent the cross-sectional area of the electric field, or if the length of the electric path is the overall distance between the electrodes or only the length of the tube. To investigate the most accurate method to estimate the solution resistance $R_Ω$ from the solution conductivity, we compared the solution resistance obtained from EIS with $R_Ω$ calculated with eq. (1) using three different approaches (Fig. 1): (1) the solution resistance calculated using the total distance between the electrodes (l) and the relative area (A) of the tube and the electrodes (Fig. 1A); (2) the distance between the electrodes considering only the cross-sectional area of the tube (Fig. 1B); and (3) using only on the length and area of the tube (Fig. 1C). The membrane resistance will be included in $R_Ω$ obtained from EIS (Fig. 1D), and the slope of the polarization curve and will not be considered in the calculation using eq. (1).

3. Results and discussion

3.1. Tube architecture is the main factor affecting the solution resistance

The small tube connecting the two bottles in H-cell MFCs is the main contributor to the solution resistance, with negligible resistance from the membrane or the solutions in the bottles (Fig. 1). The solution resistance calculated with eq. (1) using only the tube length (l_3) and area (Fig. 1C) accounted for almost the entire $R_Ω$ obtained from the EIS spectra and the slope of the polarization curve (Table S1, Table S2, Fig. S5). The calculated solution resistances using only the tube dimensions were <7% different from those obtained using EIS, with 242 Ω calculated from the tube dimensions with eq. (1), compared to 258 ± 10 Ω for the LT-MFC and 868 Ω and 860 ± 7 Ω for the ST-MFC from EIS (Fig. 1). These solution resistances are similar to those obtained from the slope of the polarization curves reported in the Supporting Information (LT-MFC = 247 ± 3 Ω and ST-MFC = 866 ± 34 Ω). Using the other two approaches shown in Fig. 1 greatly overestimated the solution resistance. For example, the solution resistance calculated using the tube area and the electrode distance (l_2) overestimated $R_Ω$ by >75% ($R_{Ω\text{-}LT}$ = 451 Ω, $R_{Ω\text{-}ST}$ = 1620 Ω), and using the areas of the electrodes to calculate the solution resistance overestimated $R_Ω$ by >24% (l_2, $R_{Ω\text{-}LT}$ = 395 Ω, $R_{Ω\text{-}ST}$ = 1066 Ω). The impact of the membrane resistance on the solution resistance was negligible based on our calculation, consistent with previous studies on microbial electrolysis cells (MECs) showing membrane resistance is small compared to the magnitude of $R_Ω$ [22,29]. For example, it was previously reported that Nafion resistance is ~1.5 Ω cm^2 [31], resulting in 1.3 Ω for the ST-MFC and only 0.3 Ω for the LT-MFC, contributing to ~0.1% to $R_Ω$ in both configurations.

3.2. Impact of tube areas on MFC power production

Decreasing the tube cross sectional area from 4.5 cm^2 to 1.2 cm^2 substantially reduced the maximum power produced by the H-cell MFCs (Fig. 2). The large tube (LT-4.5 cm^2) MFC produced a maximum power of 0.37 ± 0.00 mW, compared to only 0.13 ± 0.00 mW for the smaller tube (ST- 1.2 cm^2) MFC with the

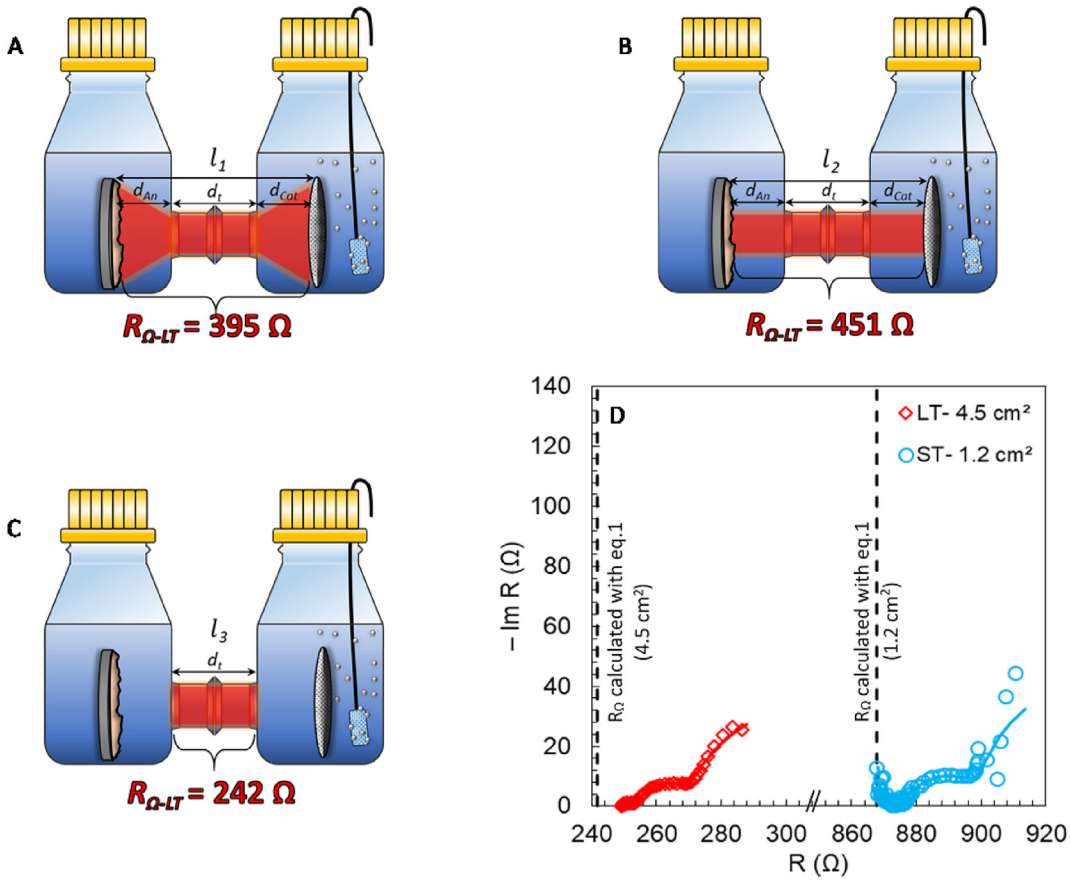

Fig. 1. (A, B, C) Three scenarios used to calculate the solution resistance (R_Ω - indicated in red). (D) EIS spectra of MFCs with 4.5 cm^2 tube (LT) and 1.2 cm^2 tube (ST) with 9.6 cm^2 anode and cathode. The vertical dashed lines represent the solution resistance calculated in 1C. The equation for calculate R_Ω and the parameters used to calculate it in A, B and C is reported in the Materials and Methods section (eq. (1)). (For interpretation of the references to colour in this figure legend, the reader is referred to the Web version of this article.)

same electrode areas (9.6 cm^2). This trend is in line with previous studies showing that smaller tube/PEM areas reduce power output [19]. The higher solution resistance (R_Ω) of the ST-MFC compared to the LT-MFC was responsible for the lower performance and the main contributor to the internal resistance of the reactor. For example, in the LT-MFC the solution resistance obtained from EIS ($R_{\Omega\text{-}LT}$ = 258 ± 10 Ω) accounted for 77% of the total internal resistance ($R_{int\text{-}LT}$ = 333 ± 3 Ω) calculated using the slopes of the polarization data (Fig. S5, Fig. S6) [15], while in the ST-MFC the impact of the solution resistance ($R_{\Omega\text{-}ST}$ = 860 ± 7 Ω) increased up to 81% of the total internal resistance ($R_{int\text{-}ST}$ = 1073 ± 34 Ω). Using more concentrated buffer solution will decrease the impact of the solution resistance to the total internal resistance. For example, with 200 mM PBS (σ = 20.0 mS cm^{-1}), the solution resistance calculated with eq. (1) will be 83 Ω for the LT-MFC, and 313 Ω for the ST-MFC.

Reducing the anode area did not appreciably impact power production until the anode projected area became smaller than the tube area (Fig. 2A and B). When the anodes were larger than the tube areas, power curves were approximately the same (<15% variation in the maximum values). However, when the anode surface area (1.8 cm^2) became smaller than tube area (4.5 cm^2) in the LT-MFC, the maximum power decreased slightly to 0.35 ± 0.00 mW compared to the 9.6 cm^2 anode (0.37 ± 0.00 mW, 9.6 cm^2). When the anode was only 0.8 cm^2 (18% of the tube area), the maximum power decreased further to 0.27 ± 0.00 mW. The power curve with the smallest anode (0.8 cm^2) showed power overshoot (a doubling back of the power curve), suggesting the biofilm was not adequately acclimated to high current [32,33]. Further acclimation of this small anode to a low external resistance increased the maximum power to 0.35 ± 0.00 mW (Fig. S7). The anode projected area was overall less critical to power production in the ST-MFC performance than in the LT-MFC, with a maximum power with a 0.8 cm^2 anode of 0.13 ± 0.00 mW, similar to that obtained with a 9.6 cm^2 anode (0.13 ± 0.00 mW, 9.6 cm^2).

Reducing the cathode area, while maintaining the anode area at 9.6 cm^2, produced small but noticeable changes in power when the cathode was larger than the tube diameter (Fig. 2C and D). However, very large changes in power were observed when the cathode became smaller than the tube. For example, P_{max} for the LT-MFC with the larger cathodes were similar, with 0.34 ± 0.00 mW (4.9 cm^2 cathode) and 0.33 ± 0.00 mW (3.1 cm^2 cathode). However, it decreased by 18% to 0.27 ± 0.00 mW for the 1.8 cm^2 cathode, and by an additional 33% to 0.18 ± 0.00 mW for the smallest cathode (0.8 cm^2) (Fig. 2C and D). The MFC with the much smaller 1.2 cm^2 tube showed less impact of the cathode dimension on the maximum power. For example, $P_{max\text{-}ST}$ decreased by only 29%, from 0.13 ± 0.00 mW (7.1 cm^2) to 0.09 ± 0.00, with the smallest cathode area (0.8 cm^2).

3.3. Impact of electrode resistance on MFC performance

The anode area had a large impact on the MFC internal resistance only when the electrode area was smaller than the tube area. For example, the anode resistance increased only from 26 ± 1 Ω to 34 ± 1 Ω by reducing the anode area from 9.6 cm^2 to 4.9 cm^2 in the LT-MFC with a tube area of 4.5 cm^2. However, decreasing the anode

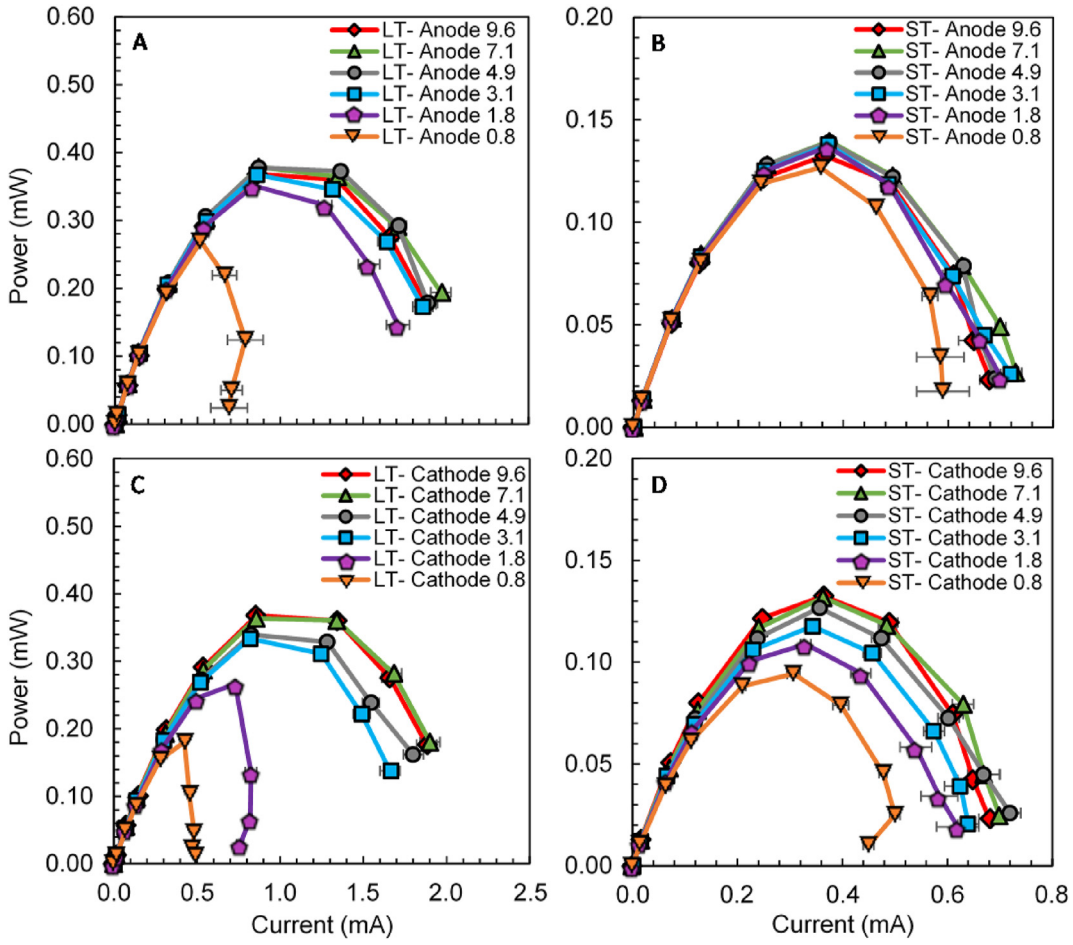

Fig. 2. (A,B) Power produced by MFCs with 4.5 cm^2 tube (LT) and 1.2 cm^2 tube (ST) and variable (A, B) anode projected areas (from 9.6 cm^2 to 0.8 cm^2) and (C, D) cathode projected areas (from 9.6 cm^2 to 0.8 cm^2).

area to 3.1 cm^2 doubled R_{An} to 50 ± 1 Ω compared to that obtained with a 9.6 cm^2 anode, and further reducing the anode area to 0.8 cm^2 increased R_{An} to 431 ± 229 Ω (Fig. 3A, Fig. S8). Reducing the anode area did not affect the cathode resistance for anode areas up to 1.8 cm^2. The cathode resistance slightly increased from 64 ± 4 Ω (1.8 cm^2 anode) to 103 ± 7 Ω (0.8 cm^2 anode) as the anode size decreased due to the lower current produced and the inclusion of a larger portion of activation losses in R_{Cat} (Fig. S11). The limited impact of the anode area on the performance of the ST-MFC was due to the large solution resistance. For example, the increase in the anode resistance by reducing the electrode area from 7.1 cm^2 to 0.8 cm^2 ($R_{An\text{-}ST}$ = 28 ± 2 Ω, 7.1 cm^2; $R_{An\text{-}ST}$ = 141 ± 3 Ω, 0.8 cm^2) accounted for less than 10% of the cathode and solution resistances ($R_{\Omega\text{-}ST}$ + $R_{Cat\text{-}ST}$ = 1074 ± 19 Ω, 7.1 cm^2 and $R_{\Omega\text{-}ST}$ + $R_{Cat\text{-}ST}$ = 1061 ± 18 Ω, 0.8 cm^2).

Cathode areas smaller than the tube area reduced the MFC performance by increasing the cathode resistance (Fig. 3B, D). $R_{Cat\text{-}LT}$ slightly increased from 61 ± 5 Ω (9.6 cm^2 cathode) to 73 ± 7 Ω (4.9 cm^2 cathode), further reducing the cathode area to 3.1 cm^2 increased $R_{Cat\text{-}LT}$ by 38% to 101 ± 5 Ω and to 1246 ± 805 Ω with the smaller cathode 0.8 cm^2. Thus, cathode areas smaller than the tube areas produced larger resistance and reduced the performance of the LT-MFC. The large impact of the electrode size on the cathode performance was likely due to the sluggish oxygen reduction reaction (ORR) on carbonaceous catalysts, and by oxygen mass-transfer, as evidenced by the comparison of diffusion in the EIS spectra (Fig. S3, Fig. S4) [34,35].

The smaller current produced in the ST-MFC reduced the impact of smaller cathode on performance. For example, $R_{Cat\text{-}ST}$ increased by <75%, from 181 ± 22 Ω (9.6 cm^2) to 317 ± 6 Ω with a 0.8 cm^2 cathode, compared to a change of 20× in the LT-MFC. The larger cathode resistance in the ST-MFC in respect to LT-MFC was due to the lower current produced by the MFC with smaller tube and the inclusion of a larger portion of activation losses in $R_{Cat\text{-}ST}$ (Fig. S11). The initial slow decrease in MFC performance even with cathode areas larger than tube areas was due to a decrease in the operative cathode potential (Fig. 1D). For example, $E_{Cat,e0}$ decreased from 508 ± 7 mV (9.6 cm^2) to 426 ± 2 mV (0.8 cm^2). This decrease was likely due to the local alkalinization of the solution near the cathode, as the ORR at neutral pH involves the production of hydroxyl ions. By decreasing the cathode area the current density increased, generating larger amounts of OH^-, and an increment of one unit of pH will decrease the cathodic potential by 59 mV, based on the Nernst equation [34,35].

In all tests, reducing the electrode projected area had negligible impact on the solution resistances measured using EIS (Fig. 3, Table S1, Table S3). R_{Ω} increased by less than 7% by decreasing the anode or cathode area from 9.6 cm^2 to 0.8 cm^2 (Table S1, Table S2). In addition, moving the electrodes further away from the tubes also did not impact current production (Fig. S12). The solution resistance was not affected by the relative area of the electrode likely because the electric field was not constrained in the anode chamber due to the large empty volume of the bottle in respect to that of the electrode. The main factors controlling R_{Ω} in H-cell MFCs is the

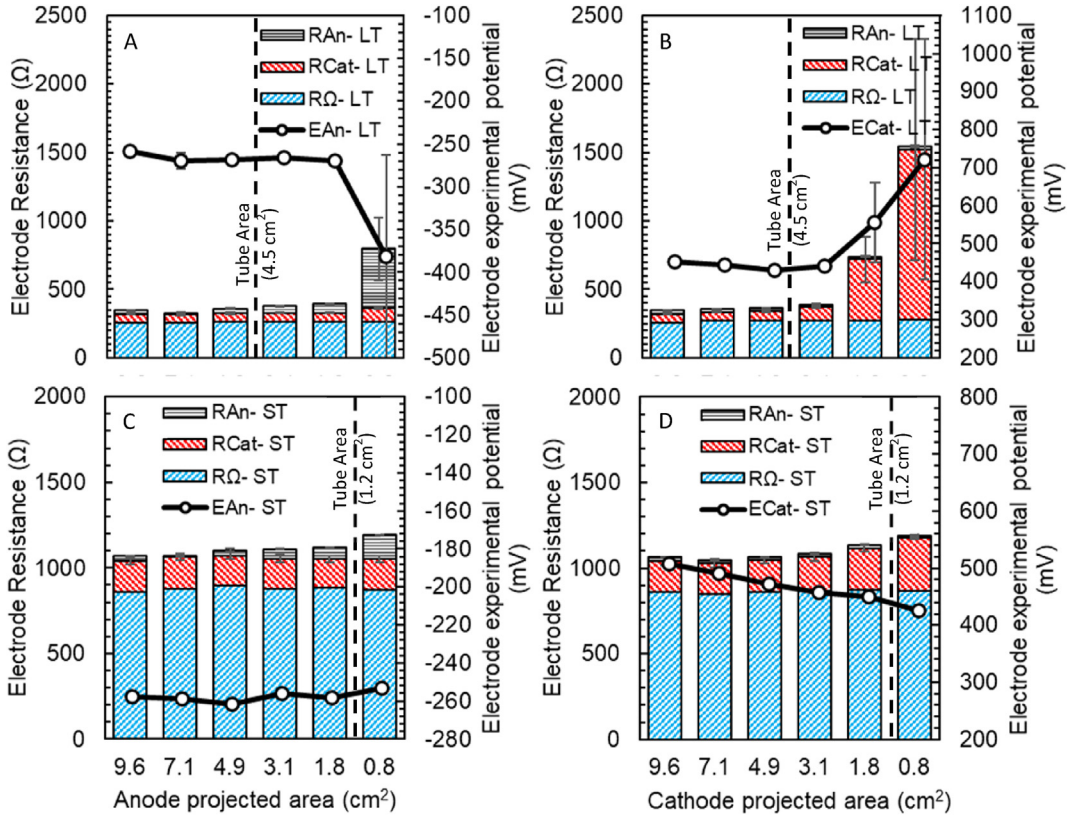

Fig. 3. Contribution of the anode (R_{An}), cathode (R_{Cat}), and solution (R_{Ω}) resistances and electrode experimental potential ($E_{An,e0}$, $E_{Cat,e0}$) in MFCs with 4.5 cm^2 tube (LT) and with 1.2 cm^2 tube (ST) and variable (A, C) anode projected areas and (B, D) cathode projected areas.

cross-sectional area of the side arm connecting the two bottle chambers, its length and the solution conductivity, independently by the electrode dimension.

3.4. Area-normalized power densities in H-Cell MFCs

Comparison of power and electrode resistances for MFCs with different electrode sizes and configurations is usually made by normalization using a single cross sectional area. When the cross sectional area is the same for the anode, cathode and membrane (if present), it does not matter which area is used. However, for H-cells, it is not clear what area should be used for calculating the power density or area normalized resistances, and therefore how to compare results of H-cells with other types of MFCs. For example, if the power in the LT-MFC was normalized using the anode area, the maximum power density would range from 383 ± 3 mW m^{-2} (anode area of 9.6 cm^2) to 3361 ± 4 mW m^{-2} (0.8 cm^2) (Fig. 4A). This power density for the small anode is much larger than that typically obtained in MFCs with electrode areas equal to that of the cross section between them [15]. If the tube cross sectional area is used to normalize the power, then the calculated power density changes as the anode size is reduced. For example, power density calculated based on tube area (4.5 cm^2) ranged from 814 mW m^{-2} for the 9.6 cm^2 anode, to 595 mW m^{-2} for the 0.8 cm^2 anode (Fig. S13).

A better method to calculate a maximum power density is proposed here based on using the results of the EPS analysis for electrode areas larger than the tube areas. The maximum power density (PD_{max}) is calculated from the experimental electrode potentials ($E_{Cat,e0}$ and $E_{An,e0}$) and the area normalized resistance (R_n, mΩ m^2) as

$$PD_{max} = \left(\frac{E_{Cat,e0} - E_{An,e0}}{2}\right)^2 \times \frac{1}{R_n} \quad (2)$$

$$R_n = R_{An}\,A_{An} + R_{Cat}\,A_{Cat} + R_{\Omega}\,A_{\Omega} \quad (3)$$

where A_{An} is the projected area of the anode, A_{Cat} the area of the cathode, and A_{Ω} the area of the tube. This approach provides a reasonable estimate of power density for the H-cell system as long as the electrodes are larger than the tube. For example, the maximum power density calculated with eq. (2) was 631 mW m^{-2} with 9.6 cm^2 anode and cathode (0.37 ± 0.00 mW), and reducing the electrode area only slightly increased the calculated power density to 685 mW m^{-2} (0.38 ± 0.00 mW) for the 4.9 cm^2 anode) and 669 mW m^{-2} (0.34 ± 0.00 mW) for the 4.9 cm^2 cathode in the LT-MFC (Fig. 4A). However, when the electrodes became very small (smaller than the tube), the calculated maximum power density increased to 752 mW m^{-2} (0.8 cm^2 anode) and 993 mW m^{-2} (0.8 cm^2 cathode), even though the actual power produced by the MFCs decreased (0.27 ± 0.00 mW, 0.8 cm^2 anode; and 0.18 ± 0.00 mW, 0.8 cm^2 cathode). Thus, calculating the maximum power density using eq. (2) gives reasonable results if the electrode area is larger than the tube area for the case of the LT-MFC.

The maximum power densities calculated using eqs. (2) and (3) were lower for the smaller tube MFC compared to that of larger tube MFC, consistent with the measured power and higher internal resistances. However, while the power densities were relatively consistent when anode was larger than the tube diameter, they were more impacted by using cathodes even when they were larger than the tube size. For example, the PD_{max} was 486 mW m^{-2} with both 9.6 cm^2 anodes and cathodes (0.13 ± 0.00 mW) with the

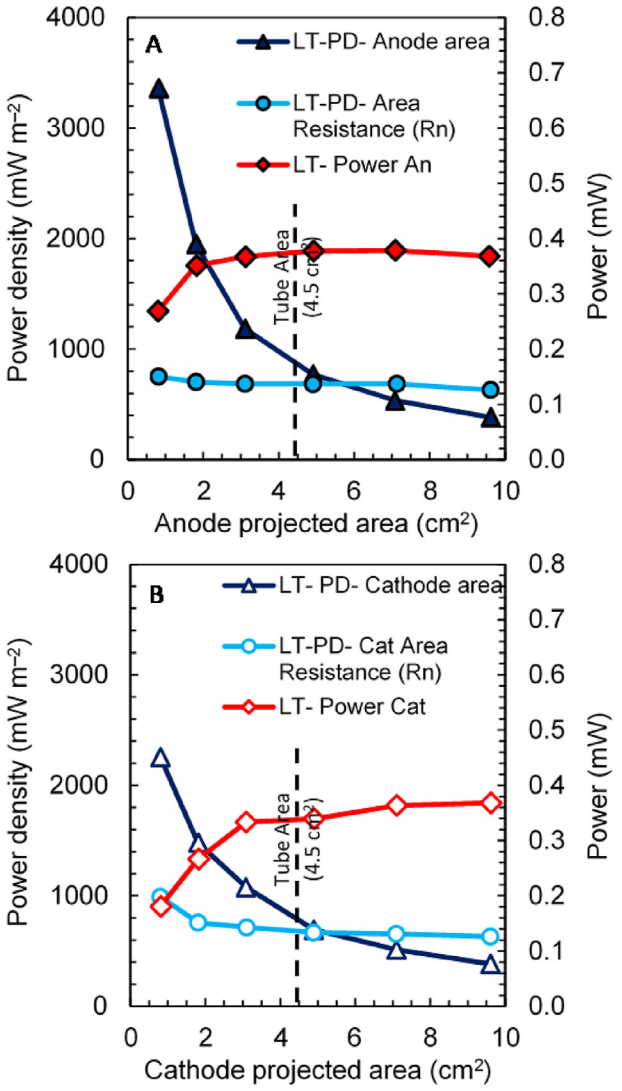

Fig. 4. Maximum power (P) and maximum power density (PD) produced by the LT-MFCs by varying the (A) anode or (B) cathode projected area normalized by the smaller electrode area or by the area-normalized resistance. The ST-MFC maximum power and power densities were reported in the Supporting Information.

1.2 cm^2 tube, and it increased only slightly to 543 mW m^{-2} when the anode was reduced to 1.8 cm^2 (0.14 ± 0.00 mW). However, with the 1.8 cm^2 cathode the calculated maximum power density increased to 733 mW m^{-2}, even though the amount of power produced by the MFC decreased (0.11 ± 0.00 mW). The reason for this increased power density with the cathode larger than the tube area was the large decrease in the area-normalized resistance of the cathode with size. For example, the cathode resistance $R_{Cat}\,A_{Cat}$ was 173 ± 21 mΩ m^2 with a 9.6 cm^2 cathode, but it decreased by 75% to 43 ± 3 mΩ m^2 for the 1.8 cm^2 cathode. This decreased the total area normalized internal resistance from R_n = 302 mΩ m^2 (9.6 cm^2 cathode) to R_n = 169 mΩ m^2 (1.8 cm^2 cathode). The anode area normalized resistance was only 25 ± 1 mΩ m^2 (9.6 cm^2 anode) and its reduction (56%, 11 ± 1 mΩ m^2 with 1.8 cm^2 anode) decreased the area normalized internal resistance by a much smaller extent (302 mΩ m^2, 9.6 cm^2 anode and 288 mΩ m^2, 1.8 cm^2 anode). Thus, reducing the cathode area had a larger impact on the power density due to its larger impact on the normalized internal resistance. This emphasizes that in studies using H-cell MFCs the electrode area should always be larger than the tube area.

The maximum power densities calculated using eq. (2) are much more reasonable when they are compared to those of single or two chamber MFCs with cross sectional areas equal to the projected areas of the electrodes. For example, the maximum power densities (using the same medium used here) in a single chamber MFC was 1708 mW m^{-2} (brush anode and 70% porosity air cathode (1709 ± 77 mW m^{-2} from polarization test) and 1404 W m^{-2} using a 30% porosity cathode (1377 ± 44 mW m^{-2} from polarization test) [15]. These maximum power densities are twice those obtained in H-cell reactors here, consistent with their smaller internal resistances in single chamber MFCs due to the lower solution resistances obtained by using closely spaced electrodes.

3.5. Recommendations for future bioelectrochemical studies

Future studies using H-cell MFCs should contain information on the cross-sectional area and length of the tube. These tube dimensions are more critical to overall system performance than distances between electrodes, as the solutions in the bottles do not contribute an appreciable amount of resistance to the overall internal resistance. This conclusion that electrode distances are not important in H-cell MFCs is different from single and two chamber MFCs that have a cross sectional area equal to that of the projected areas of the electrodes as in these systems electrode distances impact internal resistance [24,25]. In all MFC studies both electrode potentials should be monitored so that the performance of the individual electrodes can be quantified using the EPS analysis in order separately evaluate the performance of the individual electrodes. In H-cell MFCs, the relatively small tube diameter relative to the size of the chambers can accounte for most (>75%) of the total internal resistance, and thus power densities should be lower than those of single chamber MFCs with closely spaced electrodes. To maximize overall power production in H-cell type MFCs, the projected areas of the electrodes should be larger than the tube diameter, particularly for the cathode as overall performance noticeably decreases as the cathode size approaches that of the tube. When using electrodes much larger than the tube diameter, the power density for the system should be calculated using eq. (2) based on the experimental electrode potentials and the area-normalized resistances.

4. Conclusion

The EPS analysis allowed the identification and quantification of the factors limiting performance in H-cell MFCs. The solution resistance contributed to >77% of the internal resistance and was only due to the length and area of the small tube connecting the anodic and cathodic chamber with negligible contribution from the membrane or the solution in the bottle. The electrode area should be larger than the tube area to avoid large decrease in the MFC performance due to mass-transfer limitations in the cathode or poor biofilm performance on the anode and to minimize the electrode resistances. Using the electrode specific resistances to calculate the power density it was possible to compare the performance of H-cell MFCs with cubic MFCs using brush anode and air cathode and ~1 cm electrode spacing, showing power densities ~65% lower, due to the large solution resistance of the H-cell configuration.

Notes

The authors declare no competing financial interest.

Declaration of competing interest

The authors declare that they have no known competing financial interests or personal relationships that could have appeared to influence the work reported in this paper.

CRediT authorship contribution statement

Ruggero Rossi: Conceptualization, Data curation, Formal analysis, Writing - original draft, Writing - review & editing. **Bruce E. Logan:** Conceptualization, Writing - review & editing.

Acknowledgments

The research was supported by funds provided by the Environmental Security Technology Certification Program via cooperative research agreement W9132T-16-2-0014 through the US Army Engineer Research and Development Center.

Appendix A. Supplementary data

Supplementary data to this article can be found online at https://doi.org/10.1016/j.electacta.2020.136291.

References

[1] B.E. Logan, R. Rossi, A. Ragab, P.E. Saikaly, Electroactive microorganisms in bioelectrochemical systems, Nat. Rev. Microbiol. 17 (2019) 307–319, https://doi.org/10.1038/s41579-019-0173-x.
[2] X.I.N. Wang, S. Cheng, Use of carbon mesh anodes and the effect of different pretreatment methods on power production in microbial fuel cells, Environ. Res. 43 (2009) 6870–6874.
[3] B.E. Logan, B. Hamelers, R. Rozendal, U. Schröder, J. Keller, S. Freguia, P. Aelterman, W. Verstraete, K. Rabaey, Microbial fuel cells: methodology and technology, Environ. Sci. Technol. 40 (2006) 5181–5192, https://doi.org/10.1021/es0605016.
[4] H. Feng, Y. Liang, K. Guo, W. Chen, D. Shen, L. Huang, Y. Zhou, M. Wang, Y. Long, TiO_2 nanotube arrays modified titanium: a stable, scalable, and cost-effective bioanode for microbial fuel cells, Environ. Sci. Technol. Lett. 3 (2016) 420–424, https://doi.org/10.1021/acs.estlett.6b00410.
[5] S. Choi, B. Kim, I.S. Chang, Tracking of *Shewanella oneidensis* MR-1 biofilm formation of a microbial electrochemical system via differential pulse voltammetry, Bioresour. Technol. 254 (2018) 357–361, https://doi.org/10.1016/j.biortech.2018.01.047.
[6] B.E. Logan, M.J. Wallack, K.Y. Kim, W. He, Y. Feng, P.E. Saikaly, Assessment of microbial fuel cell configurations and power densities, Environ. Sci. Technol. Lett. 2 (2015) 206–214, https://doi.org/10.1021/acs.estlett.5b00180.
[7] W. Yang, K.Y. Kim, P.E. Saikaly, B.E. Logan, The impact of new cathode materials relative to baseline performance of microbial fuel cells all with the same architecture and solution chemistry, Energy Environ. Sci. 10 (2017) 1025–1033, https://doi.org/10.1039/c7ee00910k.
[8] S. Georg, I. de Eguren Cordoba, T. Sleutels, P. Kuntke, A. ter Heijne, C.J.N. Buisman, Competition of electrogens with methanogens for hydrogen in bioanodes, Water Res. 170 (2019) 115292, https://doi.org/10.1016/j.watres.2019.115292.
[9] C. Santoro, C. Arbizzani, B. Erable, I. Ieropoulos, Microbial fuel cells: from fundamentals to applications. A review, J. Power Sources 356 (2017) 225–244, https://doi.org/10.1016/j.jpowsour.2017.03.109.
[10] R. Rossi, W. Yang, L. Setti, B.E. Logan, Assessment of a metal–organic framework catalyst in air cathode microbial fuel cells over time with different buffers and solutions, Bioresour. Technol. 233 (2017) 399–405, https://doi.org/10.1016/j.biortech.2017.02.105.
[11] D. Liu, R. Wang, W. Chang, L. Zhang, B. Peng, H. Li, S. Liu, M. Yan, C. Guo, Ti_3C_2 MXene as an excellent anode material for high-performance microbial fuel cells, J. Mater. Chem. A. 6 (2018) 20887–20895, https://doi.org/10.1039/c8ta07305h.
[12] R. Wang, M. Yan, H. Li, L. Zhang, B. Peng, J. Sun, D. Liu, S. Liu, FeS_2 nanoparticles decorated graphene as microbial- fuel-cell anode achieving high power density, Adv. Mater. 30 (2018) 1800618, https://doi.org/10.1002/adma.201800618.
[13] D. Liu, Q. Chang, Y. Gao, W. Huang, Z. Sun, M. Yan, C. Guo, High performance of microbial fuel cell afforded by metallic tungsten carbide decorated carbon cloth anode, Electrochim. Acta 330 (2020) 135243, https://doi.org/10.1016/j.electacta.2019.135243.
[14] A. ter Heijne, D. Liu, M. Sulonen, T. Sleutels, F. Fabregat-Santiago, Quantification of bio-anode capacitance in bioelectrochemical systems using Electrochemical Impedance Spectroscopy, J. Power Sources 400 (2018) 533–538, https://doi.org/10.1016/j.jpowsour.2018.08.003.
[15] R. Rossi, B.P. Cario, C. Santoro, W. Yang, P.E. Saikaly, B.E. Logan, Evaluation of electrode and solution area-based resistances enables quantitative comparisons of factors impacting microbial fuel cell performance, Environ. Sci. Technol. 53 (2019) 3977–3986, https://doi.org/10.1021/acs.est.8b06004.
[16] B.E. Logan, Exoelectrogenic bacteria that power microbial fuel cells, Nat. Rev. Microbiol. 7 (2009) 375–381, https://doi.org/10.1038/nrmicro2113.
[17] R. Yamasaki, T. Maeda, T.K. Wood, Electron carriers increase electricity production in methane microbial fuel cells that reverse methanogenesis, Biotechnol. Biofuels 11 (2018) 1–10, https://doi.org/10.1186/s13068-018-1208-7.
[18] L. Wei, H. Han, J. Shen, Effects of cathodic electron acceptors and potassium ferricyanide concentrations on the performance of microbial fuel cell, Int. J. Hydrogen Energy 37 (2012) 12980–12986, https://doi.org/10.1016/j.ijhydene.2012.05.068.
[19] S.E. Oh, B.E. Logan, Proton exchange membrane and electrode surface areas as factors that affect power generation in microbial fuel cells, Appl. Microbiol. Biotechnol. 70 (2006) 162–169, https://doi.org/10.1007/s00253-005-0066-y.
[20] B.E. Logan, Essential data and techniques for conducting microbial fuel cell and other types of bioelectrochemical system experiments, ChemSusChem 5 (2012) 988–994, https://doi.org/10.1002/cssc.201100604.
[21] L. Lu, J. Gu, Z.J. Ren, Comment on "Unbiased solar H2 production with current density up to 23 mA cm^{-2} by Swiss-cheese black Si coupled with wastewater bioanode, Energy Environ. Sci. 12 (2019) 3412–3414, https://doi.org/10.1039/c9ee02592h.
[22] B.P. Cario, R. Rossi, K.Y. Kim, B.E. Logan, Applying the electrode potential slope method as a tool to quantitatively evaluate the performance of individual microbial electrolysis cell components, Bioresour. Technol. 287 (2019) 121418, https://doi.org/10.1016/j.biortech.2019.121418.
[23] B.E. Logan, E. Zikmund, W. Yang, R. Rossi, K.-Y. Kim, P.E. Saikaly, F. Zhang, Impact of ohmic resistance on measured electrode potentials and maximum power production in microbial fuel cells, Environ. Sci. Technol. 52 (2018) 8977–8985, https://doi.org/10.1021/acs.est.8b02055.
[24] Y. Fan, E. Sharbrough, H. Liu, Quantification of the internal resistance distribution of microbial fuel cells, Environ. Sci. Technol. 42 (2008) 8101–8107, https://doi.org/10.1021/es801229j.
[25] P. Liang, X. Huang, M.Z. Fan, X.X. Cao, C. Wang, Composition and distribution of internal resistance in three types of microbial fuel cells, Appl. Microbiol. Biotechnol. 77 (2007) 551–558, https://doi.org/10.1007/s00253-007-1193-4.
[26] B. Kim, I.S. Chang, Elimination of voltage reversal in multiple membrane electrode assembly installed microbial fuel cells (mMEA-MFCs) stacking system by resistor control, Bioresour. Technol. 262 (2018) 338–341, https://doi.org/10.1016/j.biortech.2018.04.112.
[27] Y. Feng, Q. Yang, X. Wang, B.E. Logan, Treatment of carbon fiber brush anodes for improving power generation in air-cathode microbial fuel cells, J. Power Sources 195 (2010) 1841–1844, https://doi.org/10.1016/j.jpowsour.2009.10.030.
[28] S. Oh, B. Min, B.E. Logan, Cathode performance as a factor in electricity generation in microbial fuel cells, Environ. Sci. Technol. 38 (2004) 4900–4904, https://doi.org/10.1021/es049422p.
[29] X. Wang, R. Rossi, Z. Yan, W. Yang, M.A. Hickner, T.E. Mallouk, B.E. Logan, Balancing water dissociation and current densities to enable sustainable hydrogen production with bipolar membranes in microbial electrolysis cells, Environ. Sci. Technol. 53 (2019) 14761–14768, https://doi.org/10.1021/acs.est.9b05024.
[30] F. Zhang, J. Liu, I. Ivanov, M.C. Hatzell, W. Yang, Y. Ahn, B.E. Logan, Reference and counter electrode positions affect electrochemical characterization of bioanodes in different bioelectrochemical systems, Biotechnol. Bioeng. 111 (2014) 1931–1939, https://doi.org/10.1002/bit.25253.
[31] R.A. Rozendal, H.V.M. Hamelers, C.J.N. Buisman, Effects of membrane cation transport on pH and microbial fuel cell performance, Environ. Sci. Technol. 40 (2006) 5206–5211, https://doi.org/10.1021/es060387r.
[32] X. Zhu, J.C. Tokash, Y. Hong, B.E. Logan, Controlling the occurrence of power overshoot by adapting microbial fuel cells to high anode potentials, Bioelectrochemistry 90 (2013) 30–35, https://doi.org/10.1016/j.bioelechem.2012.10.004.
[33] B. Kim, J. An, I.S. Chang, Elimination of power overshoot at bioanode through assistance current in microbial fuel cells, ChemSusChem 10 (2017) 612–617, https://doi.org/10.1002/cssc.201601412.
[34] S.C. Popat, D. Ki, B.E. Rittmann, C.I. Torres, Importance of OH^- transport from cathodes in microbial fuel cells, ChemSusChem 5 (2012) 1071–1079, https://doi.org/10.1002/cssc.201100777.
[35] S.C. Popat, C.I. Torres, Critical transport rates that limit the performance of microbial electrochemistry technologies, Bioresour. Technol. 215 (2016) 265–273, https://doi.org/10.1016/j.biortech.2016.04.136.